

**Supplementary information to**

**Observation-based assessment of stratospheric fractional release, lifetimes, and Ozone Depletion Potentials of ten important source gases**

**J. C. Laube<sup>1</sup>, A. Keil<sup>2</sup>, H. Bönisch<sup>2</sup>, A. Engel<sup>2</sup>, T. Röckmann<sup>3</sup>, C. M. Volk<sup>4</sup> and W. T. Sturges<sup>1</sup>**

[1] {School of Environmental Sciences, University of East Anglia, Norwich, United Kingdom}

[2] {Institute for Atmospheric and Environmental Sciences, University of Frankfurt, Germany}

[3]{Institute for Marine and Atmospheric Research, Utrecht University, Netherlands}

[4]{Department of Physics, University of Wuppertal, Germany}

**Additional authors for this supplement:**

**P. J. Fraser<sup>5</sup> and D. E. Oram<sup>6</sup>**

[5]{Centre for Australian Weather and Climate Research, Commonwealth Scientific and Industrial Research Organisation, Aspendale, Victoria 3195, Australia}

[6]{National Centre for Atmospheric Science, School of Environmental Sciences, University of East Anglia, Norwich, United Kingdom}

Correspondence to: J. C. Laube (j.laube@uea.ac.uk)

Below please find additional information on Fractional Release Factors (FRFs) and the polynomials fitted to the data to calculate FRFs from mean ages of air (Table S1) as well as the methodology and parameters used to calculate the stratospheric lifetimes (Table S2).

Displayed in Figures S1 to S3 are time series of mixing ratios as measured on samples collected at a remote ground-based station at Cape Grim, Tasmania (40.4°S, 144.4°E) which have been used to investigate the comparability of measurements made by the two laboratories (i.e. NOAA-ESRL and UEA). Agreement within measurement uncertainties was found for eight compounds, but consistent offsets were identified for CFC-113 (+2 %, UEA minus NOAA), HCFC-142b (-2 %) and CH<sub>3</sub>CCl<sub>3</sub> (+4 %) using these time series. All UEA & Ufra data was corrected accordingly. The respective data set on H-1211 and H-1301 can be found in Newland et al. (2012).

Figures S4 to S12 show the slopes of the tracer-CFC-11 correlations against average CFC-11 mixing ratios. As has been noted by Volk et al. (1997) curvature of these correlations may result from local sources and sinks, local growth, and perhaps changes in the fluxes across the tropical/mid-latitude barrier. In particular, strong tropospheric growth results in positive local growth, which is equivalent to a local sink and thus expected to create an upward concavity in the correlations (assuming the effect of the small negative CFC-11 growth to be negligible). We indeed find strong curvatures of the correlations in the expected direction for CH<sub>3</sub>CCl<sub>3</sub> (very strong negative growth), HCFC-142b, and HCFC-22 (strong growth in combination with long lifetimes). For the other compounds local growth is expected to have less influence on the shape of the correlations because growth rates are small and/or the lifetimes are shorter such that stratospheric decline is dominated by chemistry. The upward concavity of the H-1211/CFC-11-correlation is most likely due to the sink of H-1211 being significant already in the lowermost stratosphere. The curvatures of the correlations for the other species are barely significant; they may be attributed to a complex interplay of (small) local sinks and growth of the respective species and of CFC-11, in combination with variable fluxes across the tropical/mid-latitude barrier.

Prior to calculations data that could have been influenced by the polar vortex was excluded (similarly to the method used for the correlation of CFC-11 and mean-age). Similar to Volk et al. (1997) the slopes were measured using error-weighted bivariate linear regression (Cantrell, 2008) fitted over windows of 70 ppt of CFC-11 and moving these windows in 5 ppt steps. The only exception was CCl<sub>4</sub> which has the smallest data set and where 90 ppt windows were used as a consequence. Also following Volk et al. (1997) the windows were narrowed slightly (down to widths of 50 ppt) in the vicinity of the tropopause. Finally the slope at the tropopause was determined by fitting error-weighted quadratic polynomials from 120 to 220 ppt of

CFC-11 and extrapolating them to the chemical tropopause at 241.0 ppt.of CFC-11. Statistical uncertainties of these slopes were determined in the same way as described in Volk et al. (1997), i.e. by repeating each fit many (here: 10,000) times with random bootstrap samples (drawing with repeat from the data set), and scaling the resulting standard deviation by a factor (square root of the number of fitted points over the number of fully independent points) to account for the interdependency of the individual slope points.

Table S1. Parameters of polynomials of the form  $y = a + bx + cx^2$  to calculate FRFs (y) from mean ages (x) as derived from mid (ml) and high latitudinal (hl) correlations. FRFs were fitted between 0 and 5.8 years of mean age but not forced through 0 as small negative numbers may occur due to atmospheric variability in the vicinity of the tropopause. Squared Pearson correlation coefficients were  $> 0.95$  except for HCFC-142b (0.90).

Compound	<i>a</i>	<i>b</i>	<i>c</i>
CFC-11 (ml)	-0.0173	0.098666	0.00816955
CFC-11 (hl)	-0.0203	0.120582	0.00644101
CFC-113 (ml)	-0.0059	0.049669	0.00862413
CFC-113 (hl)	0.0035	0.052307	0.01071417
CFC-12 (ml)	-0.0154	0.046244	0.00707356
CFC-12 (hl)	-0.0111	0.052939	0.00833816
HCFC-141b (ml)	-0.0635	0.050362	0.00939938
HCFC-141b (hl)	-0.0513	0.057713	0.01108315
HCFC-142b (ml)	-0.0032	0.010130	0.00233185
HCFC-22 (ml)	-0.0190	0.021203	0.00229434
HCFC-22 (hl)	-0.0193	0.022367	0.00349756
H-1301 (ml)	-0.0185	0.061608	0.01051828
H-1301 (hl)	-0.0336	0.086124	0.00949226
H-1211 (ml)	-0.0535	0.204371	-0.00464644
H-1211 (hl)	-0.0482	0.218376	-0.00664831
CCl <sub>4</sub> (ml)	-0.0139	0.131338	0.00464806
CCl <sub>4</sub> (hl)	-0.0326	0.154912	0.00135110
CH <sub>3</sub> CCl <sub>3</sub> (ml)	-0.0227	0.254820	-0.01505946
CH <sub>3</sub> CCl <sub>3</sub> (hl)	0.0014	0.261897	-0.01631929

Table S2. Average atmospheric mixing ratios  $\bar{\sigma}$ , effective linear growth rates  $\gamma_0$  and slopes of the correlations against CFC-11 at the tropopause  $d\chi/d\chi_{\text{CFC-11}}$  (i.e. at  $[\text{CFC-11}] = 241.0$  ppt).

Compound	$\bar{\sigma}$ [ppt]	$\gamma_0$ [% yr <sup>-1</sup> ]	$d\chi/d\chi_{\text{CFC-11}}$
CFC-11	$227.9 \pm 3.8$	-0.88	1
CFC-113	$72.5 \pm 0.9$	-0.90	$0.223 \pm 0.026$
CFC-12	$510.9 \pm 6.0$	-0.51	$1.339 \pm 0.157$
HCFC-141b	$19.1 \pm 0.3$	2.61	$0.0687 \pm 0.0224$
HCFC-142b	$19.0 \pm 0.2$	5.26	$0.0623 \pm 0.0088$
HCFC-22	$195.1 \pm 1.9$	3.86	$0.658 \pm 0.068$
H-1301	$2.98 \pm 0.04$	0.77	$0.0113 \pm 0.0005$
H-1211	$3.81 \pm 0.10$	-1.59	$0.0277 \pm 0.0033$
CCl <sub>4</sub>	$82.77 \pm 1.5$	-1.59	$0.398 \pm 0.063$
CH <sub>3</sub> CCl <sub>3</sub>	$7.7 \pm 0.1$	-21.06	$0.0266 \pm 0.0088$

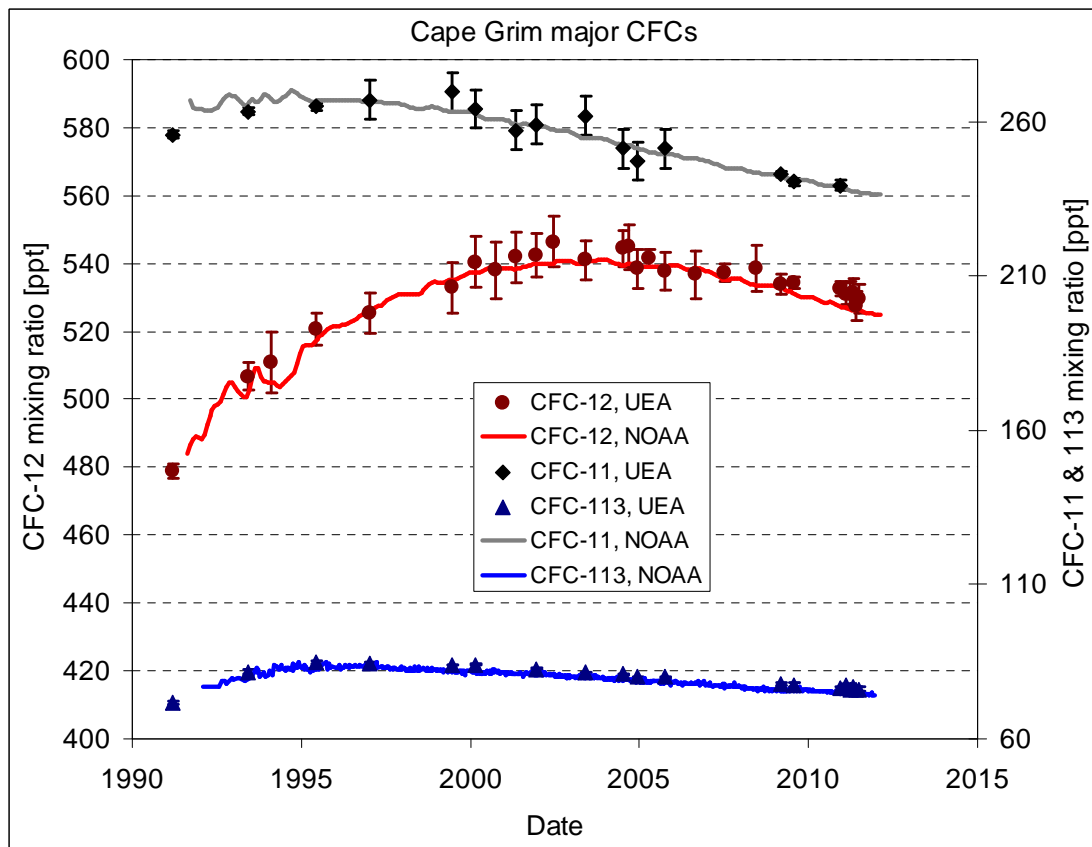


Figure S1. Comparison between mixing ratios of CFC-11, CFC-113, and CFC-12 as observed at the remote ground-based station at Cape Grim, Tasmania by the NOAA Global Monitoring division (lines) and UEA (symbols representing individual samples) between 1991 and 2011.

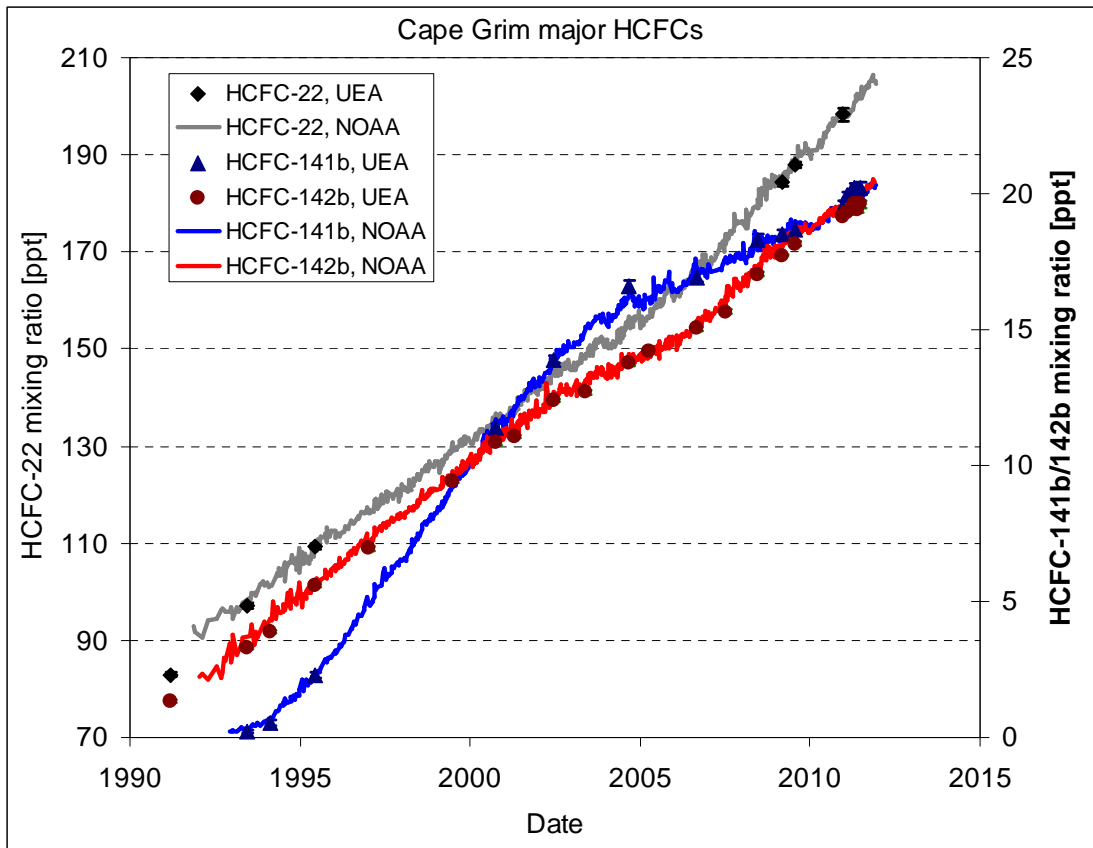


Figure S2. The same as in Figure S1 but for HCFC-141b, HCFC-142b, and HCFC-22.

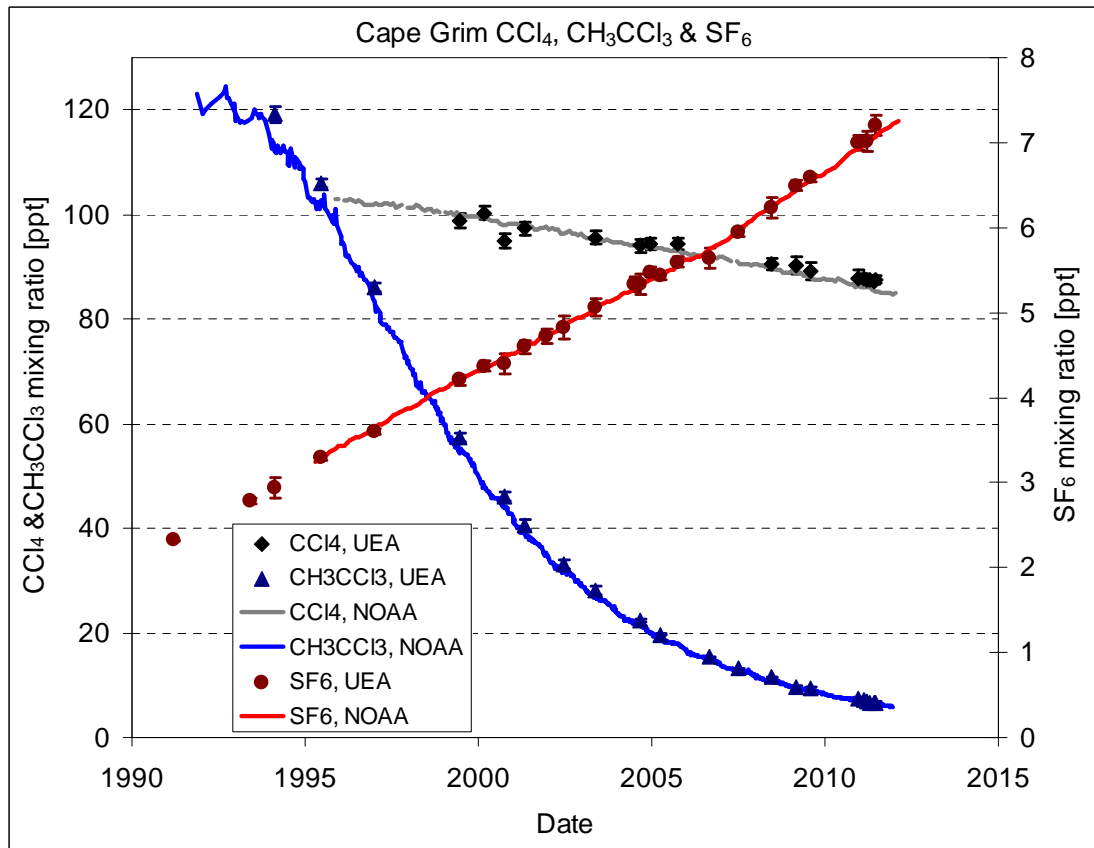


Figure S3. The same as in Figure S1 but for  $\text{CCl}_4$ ,  $\text{CH}_3\text{CCl}_3$ , and  $\text{SF}_6$ .

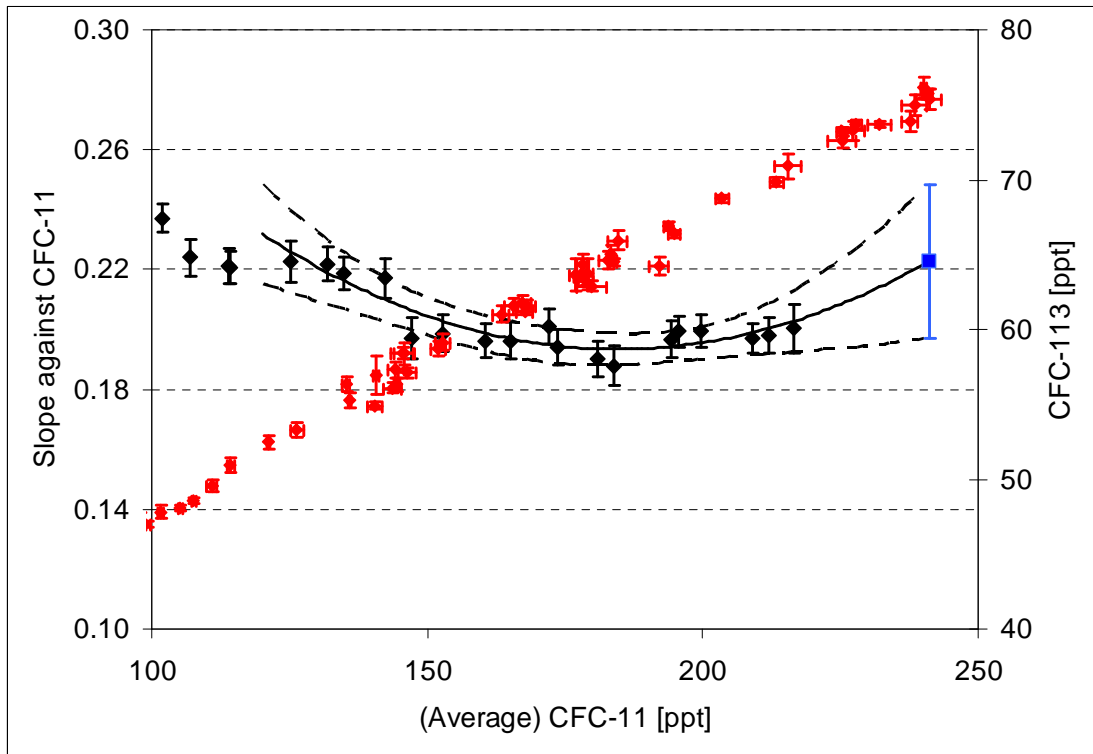


Figure S4. Evolution of correlation slopes of the mixing ratios of CFC-113 against the average mixing ratio of CFC-11. The black diamonds each represents the bivariate error-weighted slope of the correlation inferred over a range of  $\pm 35$  ppt CFC-11. The error bars represent the  $1 \sigma$  slope uncertainties. The black lines are the error-weighted quadratic polynomial fitted between 120 and 220 ppt and its respective uncertainty envelopes as inferred via the “bootstrap” method from Volk et al., 1997. Extrapolation of these polynomials to the tropopause at 241.0 ppt of CFC-11 results in the slopes and uncertainties (blue) given in Table S2. Note, that only data from the campaigns in late 2009 and early 2010 are combined for the calculation of these slopes. Displayed in red is the correlation of mixing ratios that was utilised to infer the slopes. Finally, in contrast to the slope evolution of the correlation of CFC-11 with mean age (linear regression line fitted, see Figure 1 in the main manuscript) a quadratic polynomial was fitted here as we observe more complex curvatures

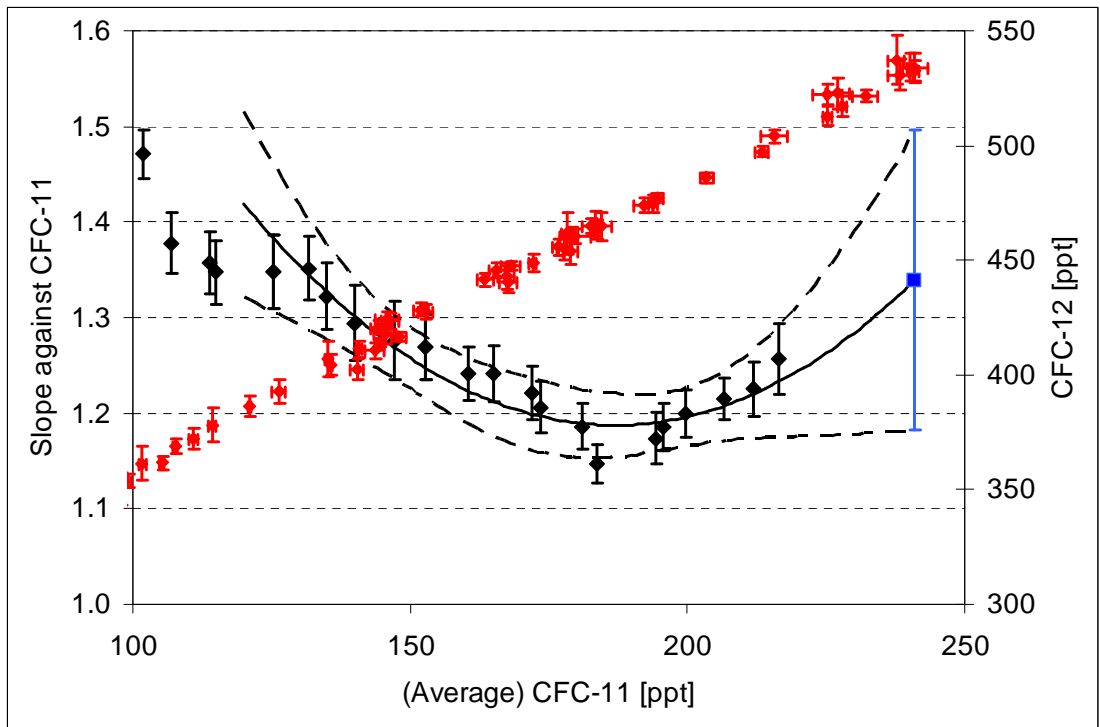


Figure S5. The same as in Figure S4 but for CFC-12.

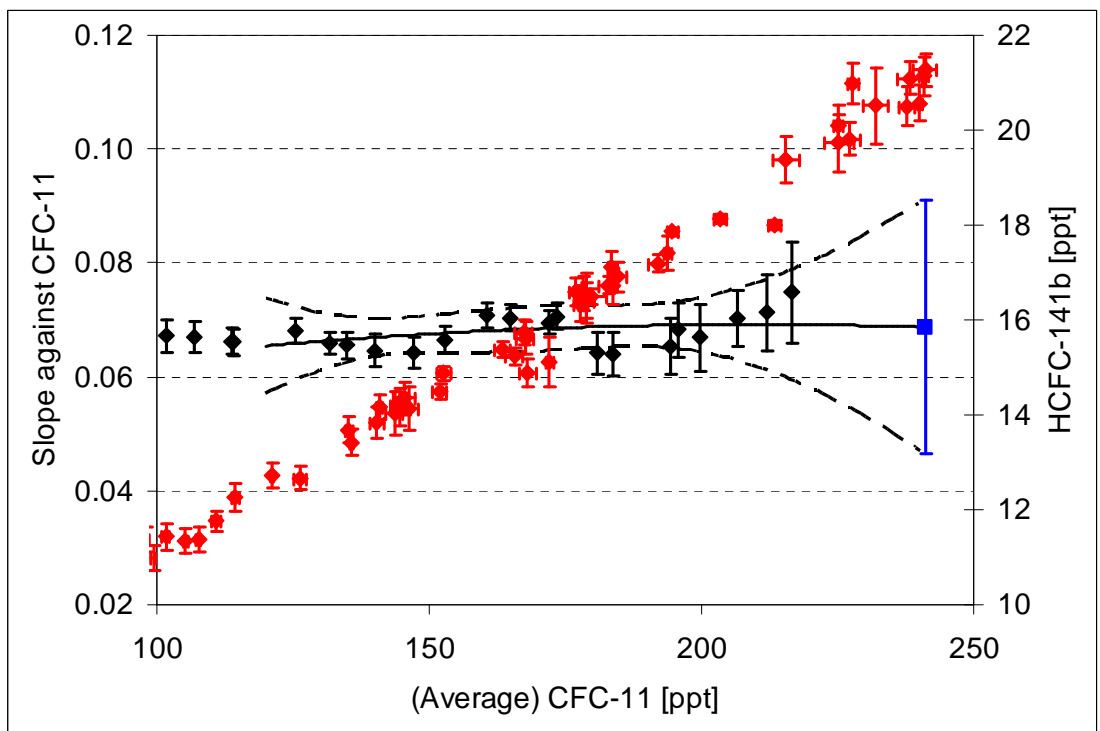


Figure S6. The same as in Figure S4 but for HCFC-141b.

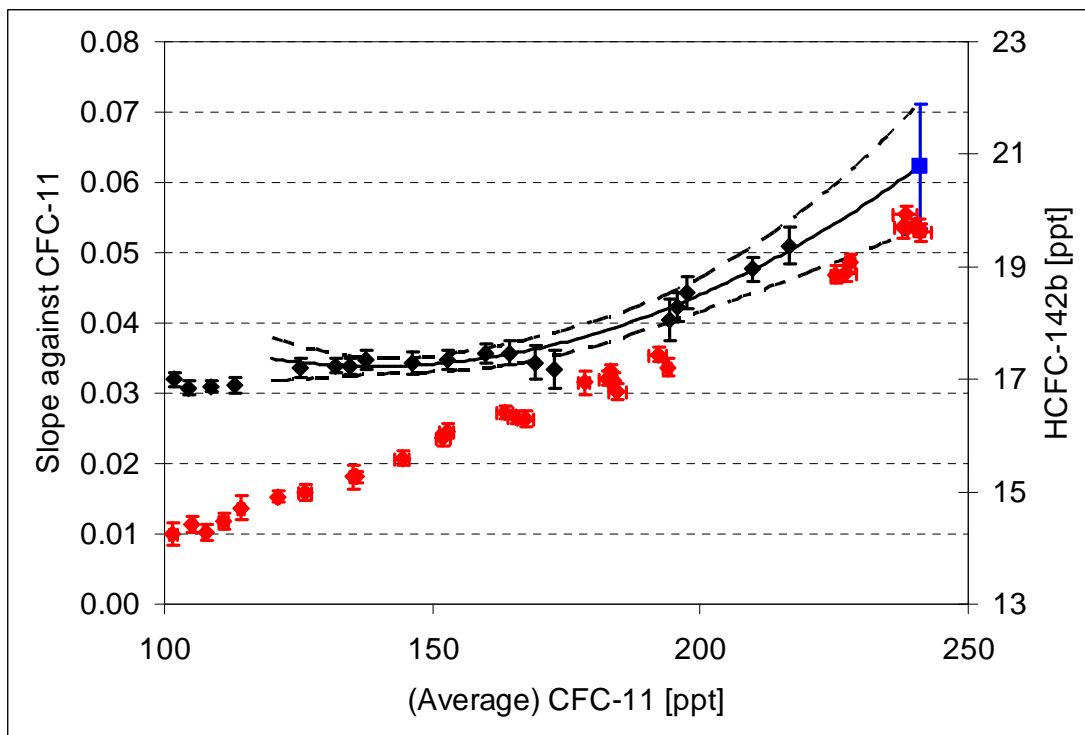


Figure S7. The same as in Figure S4 but for HCFC-142b.

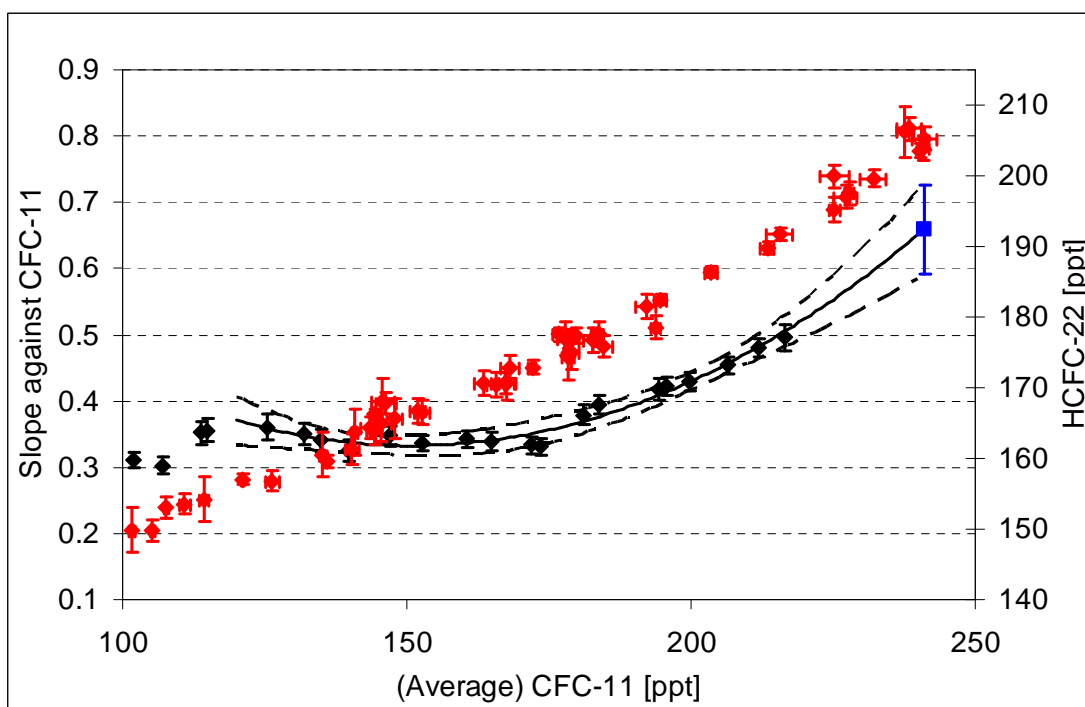


Figure S8. The same as in Figure S4 but for HCFC-22.

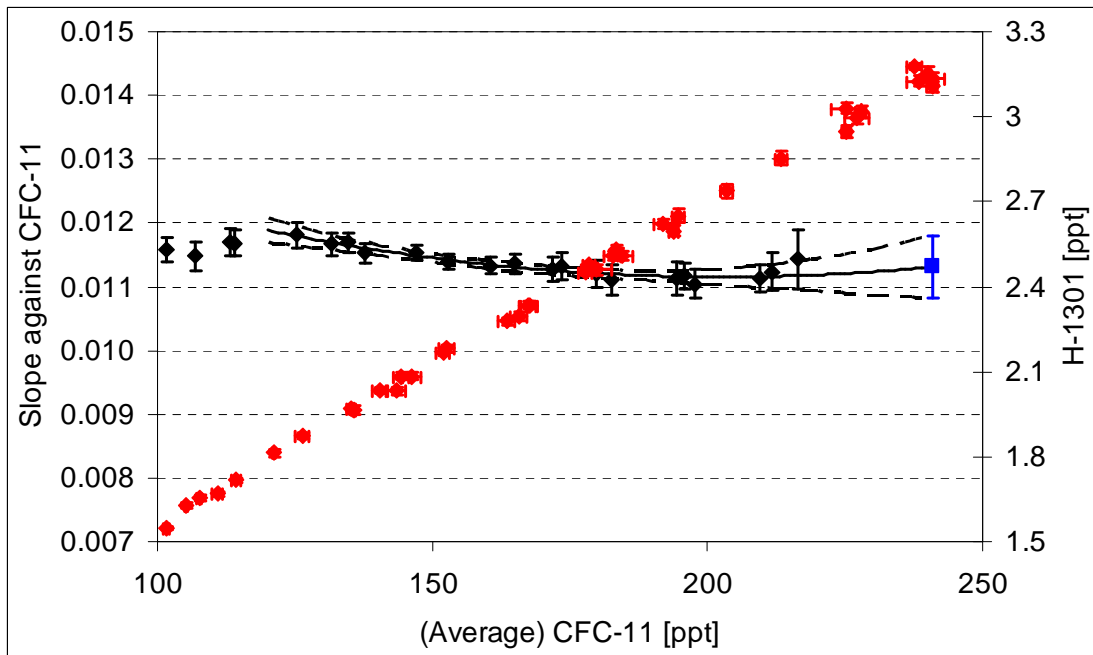


Figure S9. The same as in Figure S4 but for H-1301.

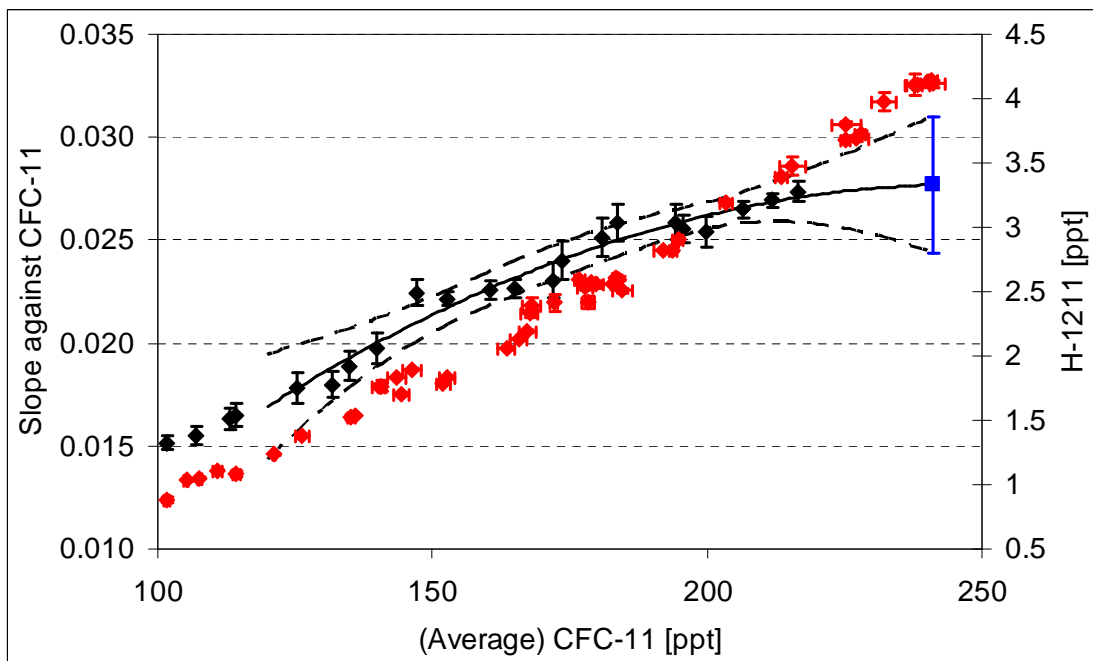


Figure S10. The same as in Figure S4 but for H-1211.

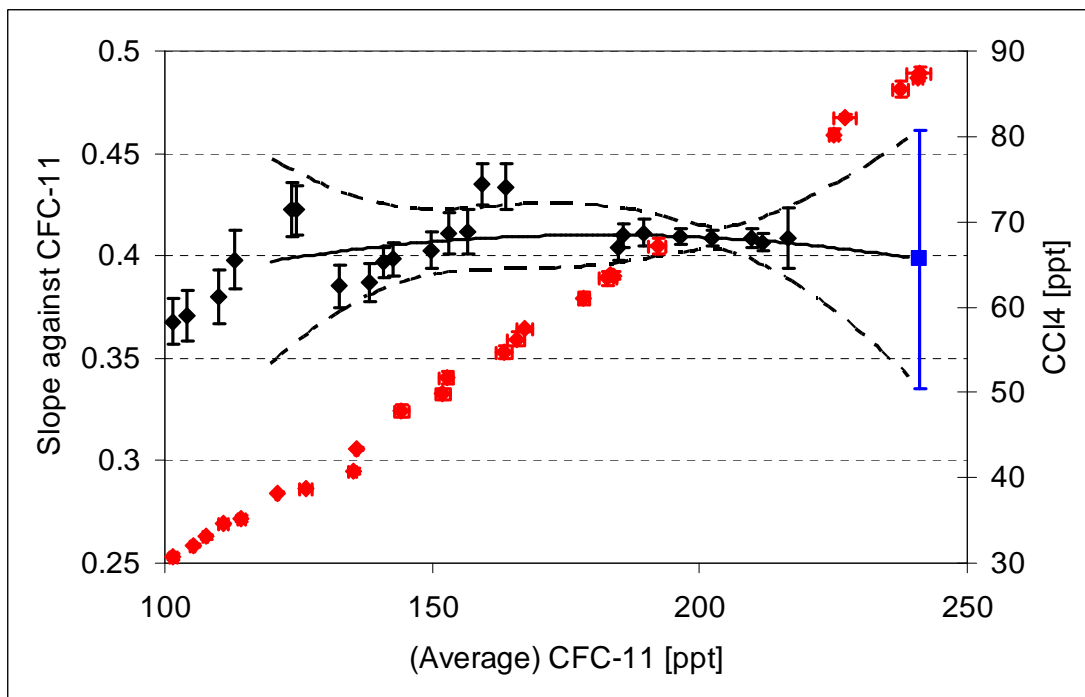


Figure S11. The same as in Figure S4 but for  $\text{CCl}_4$ . 90 ppt windows of CFC-11 were used here to infer the individual slopes.

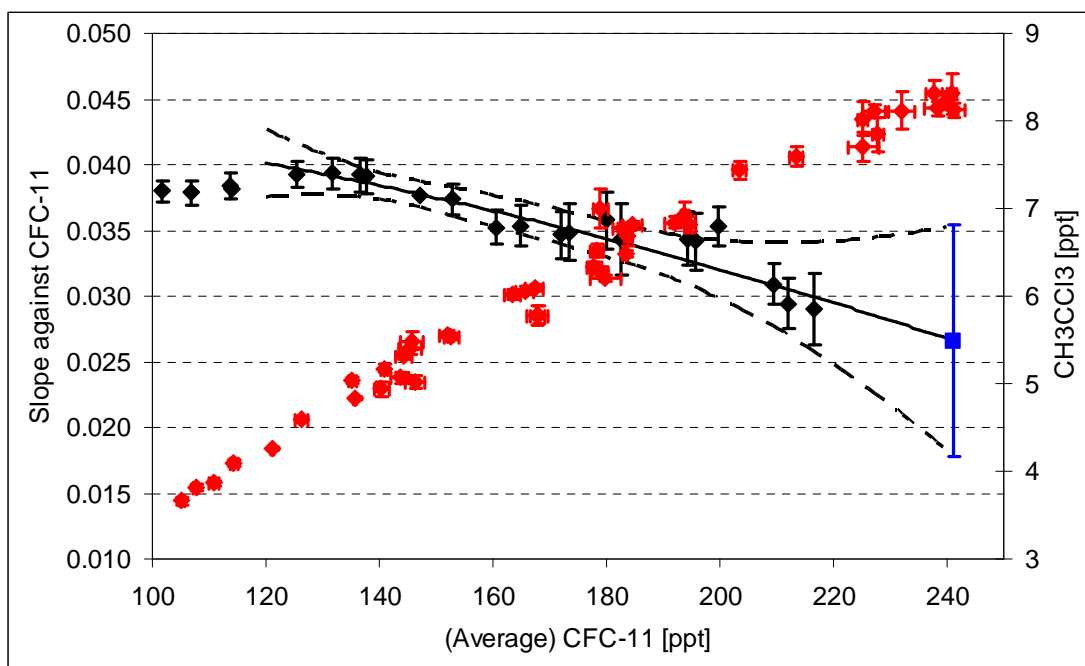


Figure S12. The same as in Figure S4 but for  $\text{CH}_3\text{CCl}_3$ .